Nanotechnology 33 (2022) 125706 (8pp) https://doi.org/10.1088/1361-6528/ac40bd

How high is a $MoSe_2$ monolayer?

Megan Cowie[1,*], **Rikke Plougmann**[1,3], **Yacine Benkirane**[1], **Léonard Schué**[2], **Zeno Schumacher**[1,4] and **Peter Grütter**[1]

[1] Department of Physics, McGill University, 3600 Rue University, Montréal, Québec H3A 2T8, Canada
[2] Département de Chimie and Regroupement Québécois sur les Matériaux de Pointe (RQMP), Université de Montréal, C.P. 6128, Succursale Centre-Ville, Montréal, Québec H3C 3J7, Canada

E-mail: mecj.cowie@gmail.com

Received 13 September 2021, revised 29 November 2021
Accepted for publication 7 December 2021
Published 28 December 2021

Abstract

Transition metal dichalcogenides (TMDCs) have attracted significant attention for optoelectronic, photovoltaic and photoelectrochemical applications. The properties of TMDCs are highly dependent on the number of stacked atomic layers, which is usually counted post-fabrication, using a combination of optical methods and atomic force microscopy height measurements. Here, we use photoluminescence spectroscopy, Raman spectroscopy, and three different AFM methods to demonstrate significant discrepancies in height measurements of exfoliated $MoSe_2$ flakes on SiO_2 depending on the method used. We also highlight the often overlooked effect that electrostatic forces can be misleading when measuring the height of a $MoSe_2$ flake using AFM.

Supplementary material for this article is available online

Keywords: molybdenum diselenide (MoSe2), Transition metal dichalcogenides (TMDCs), 2D materials, atomic force microscopy (AFM), photoluminescence spectroscopy (PL), kelvin probe force microscopy (KPFM), Raman spectroscopy

(Some figures may appear in colour only in the online journal)

1. Introduction

Transition metal dichalcogenides (TMDCs) are of increasing interest as promising contenders for a wide range of optoelectronic and electrochemical applications due to their strong light–matter interactions, tunable optical bandgaps and flexible two-dimensional (2D) structure [1, 2]. Molybdenum diselenide ($MoSe_2$) is one of the most promising TMDC candidates for photoelectrochemical energy conversion due to its photocatalytic properties and the electrical conductivity of Se [1, 3]. $MoSe_2$ monolayers have a hexagonal crystal structure that consists of top and bottom Se layers sandwiching a Mo layer [4]. Stacked $MoSe_2$ layers are weakly coupled via van der Waals coupling [5] and have an interlayer spacing in bulk of 0.65 nm [6–10]. For both fundamental studies and device functionality, it is vital to be able to confirm the number of layers present in TMDC samples, because the number of stacked atomic layers in TMDC samples can drastically affect their properties [4, 11, 12]. In addition, it is important to understand how the properties of the different layers in stacked TMDC structures could be influenced during fabrication and from interactions with the underlying substrate [13].

As with other 2D materials, TMDC layers can be synthesized both via chemical vapor deposition (CVD) [14–16] and, most commonly, using mechanical exfoliation [1, 2, 11, 13, 17–20], in which mono- or few-layer flakes are transferred onto a substrate, often SiO_2/Si. E. Pollman *et al* [13] carried out a study on MoS_2 comparing the properties of samples fabricated by both techniques, and demonstrated the presence of intercalated water on exfoliated monolayers, leading to both an increased step height and a decreased intensity in photoluminescence spectroscopy [13]. A further challenge is that samples are often handled in air, leading to airborn contaminants [21]. $MoSe_2$ has been shown to be particularly susceptible to surface contaminants as compared to sulfur-based TMDCs [21], but both exhibit discrepancies in

[3] Present address: Department of Physics, Technical University of Denmark, Fysikvej, Building 311, 2800 Kgs. Lyngby, Denmark.
[4] Present address: Institute of Quantum Electronics, ETH Zürich, Auguste-Piccard-Hof 1, 8093 Zürich, Switzerland.
[*] Author to whom any correspondence should be addressed.

 © 2021 IOP Publishing Ltd Printed in the UK

height measurements, ranging from the approximately 0.7 nm [22, 23] expected given the crystallographic structure [6–10] to much larger values [1, 17, 20, 24, 25]. Given this lack of consensus, it is imperative to understand how contaminants and other effects may influence the height profile measurements for $MoSe_2$.

1.1. Methods for counting layers

The number of layers present in TMDC samples is usually measured using a combination of optical microscopy [26, 27], photoluminescence spectroscopy (PL) and/or Raman spectroscopy together with step height measurements made by atomic force microscopy (AFM) [14, 28–30]. In optical microscopy images, the contrast difference between layers can be analyzed for the red, green and blue channels of the image [12, 31, 32]. AFM is used to measure the height of a flake, and comparing that to the expected interlayer spacing of the 2D material. There is much discrepancy among AFM height measurements of mechanically exfoliated TMDCs on SiO_2: some show heights between 0.65 and 1.0 nm [19, 20, 29] while others are much larger, ranging between 2 and 3 nm [17, 24]. Elevated heights are often attributed to surface contaminants [1, 17, 20, 25]. Raman spectroscopy is also common TMDC characterization method. With this technique, layer numbers can be determined based on the layer-dependent shift in the energy levels of the phonon modes [33].

PL is another widely used technique used to characterize TMDC layer numbers. The position of the monolayer peak in a PL spectrum for exfoliated $MoSe_2$ samples has been observed at room temperature in the range 788–816 nm [5, 14, 15, 20, 28, 34–36]. The PL intensity can be affected by the presence of defects [16] and adsorbates [28] and is expected to decrease as the number of layers increases [5, 20, 28, 37]. There is a lack of consensus in the literature regarding how to interpret PL spectra for 2, 3, and N layers of $MoSe_2$. For $MoSe_2$ flakes mechanically exfoliated onto SiO_2, P. Tonndorf *et al* [28] show a 15nm redshift of the dominant A peak for a bilayer and significant broadening and flattening of the A peak for 3 layers. In contrast, Y. Sha *et al* [20] measured only a few nm redshift as the number of $MoSe_2$ layers increases. S. Tongay *et al* [37] also show a negligible shift in position of the peak as the number of $MoSe_2$ layers increases from 1 to 3 layers. In some cases, observations from bilayers have exhibited the properties of a monolayer, which is thought to be due to the formation of pockets between the layers during exfoliation [29]. The degree of coupling between exfoliated $MoSe_2$ layers has been shown to significantly influence their photoluminescence, as demonstrated by S. Tongay *et al* using thermally controlled coupling [37].

In this work, two $MoSe_2$ flakes were measured using optical microscopy, Raman spectroscopy, PL spectroscopy and three different modes of AFM: tapping mode, non-contact AFM (nc-AFM) and Kelvin probe force microscopy (KPFM). The presence of electrostatic forces can significantly influence the topographic height profile measured using nc-AFM [38, 39]. In KPFM, the net electrostatic force is minimized using a feedback loop to apply a DC bias, and KPFM thereby provides information about contact potential variations over the sample surface, either due to non-homogeneities in the sample material or localized charging or polarization effects [40–42].

2. Results & discussion

$MoSe_2$ flakes were transferred onto a substrate of SiO_2 using all-dry viscoelastic stamping [26]. Figure 1 provides an overview of the sample regions that were selected for study. Flake 1 is the largest, most visibly transparent area of the sample, and Flake 2 is a small island that has stepped layers. Figure 1(a) shows a grayscale image of the red channel of the R, G, B channels of the color optical image (the red channel is selected here as it shows the highest degree of contrast between the layers). Figures 1(b)–(d) and (e)–(g) show tapping mode, nc-AFM, and KPFM z-channel images of Flake 1 and Flake 2 respectively. The data in the KPFM z-channel images is the z-height measured after compensating for the contribution of the net electrostatic force to the height data with a standard KPFM feedback controller [40–42].

In the nc-AFM scan in figure 1(f), Flake 2 appears to be stepped, with an overlayer of some additional features on the top layer. Similar features have been observed in exfoliated $MoSe_2$ samples [21], and were attributed to airborne contamination specific to $MoSe_2$, as compared to sulfur-based TMDCs. These features are absent on the large Flake 1, potentially indicating that they are multilayer-specific, or a causal consequence of the way in which the small Flake 2 was exfoliated. The apparent stepped layers and overlayer have been labeled L1, L2, L3, and L4 (note that these regions do not necessarily correspond to 1, 2, 3, and 4 atomic layers). Figures 1(h)–(i) show the height measurements extracted from the AFM images, which are presented in tabular form on page 4 of the Supplementary Materials.

Comparing the optical contrast difference between Flake 1 and the substrate (values given for the color, green and blue channels on page 2 of the Supplementary Materials) for both the color image and red channel image to observations of other TMDCs (MoS_2 and WSe_2) on 300 nm SiO_2/Si [43], the contrast of Flake 1 agrees with that of a monolayer rather than two stacked layers. However, a definite determination of the layer count based on optical contrast is difficult for a sample that is not consisting of large flakes of 1, 2, 3, ..., N layers, where the transmittances from each flake can be compared relative to each other [31]. L. Ottaviano *et al* [17] demonstrated for MoS_2, that optical microscopy data alone can be misleading, as the contrast depends on the exact thickness of the SiO_2 layer on Si/SiO_2 samples, and is not always a monotonic function of the layer number [17]. Optical microscopy could not be used to reliably characterize Flake 2 because it has dimensions smaller than the diffraction limit of light—another limitation of determining layer number by optical contrast [17].

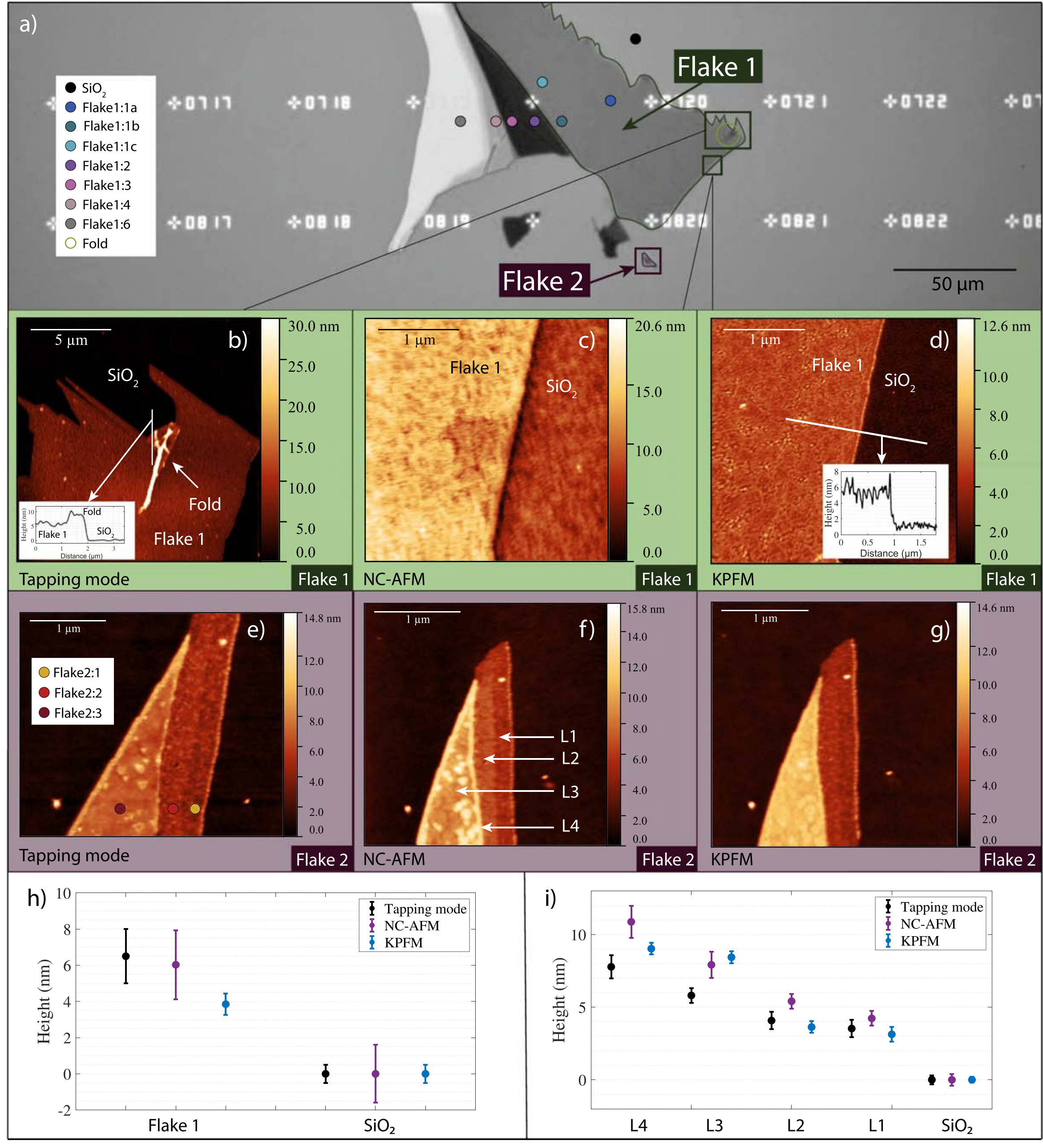

Figure 1. (a) Optical microscopy image (red channel) of the $MoSe_2$ sample. Tapping mode, nc-AFM, and KPFM images of Flake 1 (b)–(d) and Flake 2 (e)–(g). (h)–(i) show the height measurements extracted from the AFM images shown. The height measurements were extracted from the images by averaging the height over large areas in each layer, and comparing to the substrate background. The vertical error bars are the standard deviations of the heights of these large areas, added in quadrature with the substrate height standard deviation. The details of the analysis are given on page 3 of the Supplementary Materials. The coloured points in (a) and (e) indicate the locations where Raman and PL spectroscopy were performed. The details of these experiments are found in following sections.

2.1. Thickness analysis with AFM

The apparent AFM heights, shown in figures 1(h)–(i), were measured by averaging large areas of the AFM images shown in figures 1(b)–(g). Area averaging provides more robust, quantitative height measurements than individual line scans. See page 3 of the Supplementary Materials for more information as well as the results of figures 1(h)–(i) presented in tabular form. Figures 1(h)–(i) show that the height measurements of each AFM mode—tapping, nc-AFM and KPFM—often do not agree within uncertainty. This is because each mode provides different information about the sample properties, such as mechanical rigidity and electrostatic non-uniformity [41]. The net AFM force is due to a combination of forces, principally van der Waals and electrostatic. Therefore, if the electrostatic nature of a sample is spatially non-uniform (due to, for example, charging) this will lead to apparent height differences that do not reflect the topography of the surface. Therefore, when measuring sample heights with AFM, it is critical to compensate for these forces with KPFM [41, 42]. For example, the step height between the

substrate and Flake 1 in the KPFM scan (3.9 ± 0.6 nm) is significantly smaller than in the tapping mode (6.5 ± 1.5 nm) and nc-AFM (6.0 ± 1.9 nm) scans, suggesting that electrostatic forces inflate the height measurements when they are not compensated for. Note, however, that standard KPFM assumes a constant capacitive gradient between the tip and sample, which is not the case for semiconductors [44]. Therefore, even with a KPFM controller the electrostatic forces may not be completely nulled. Tapping mode is operated in a larger tip-sample force regime than nc-AFM and KPFM, so it is much more likely to mechanically influence (e.g. compress) the sample. For example, the systematically lower heights measured with tapping mode on Flake 2 could be explained by mechanical compression of an overlayer or underlayer.

For each AFM mode, the substrate:Flake 1 and substrate: L1 heights measured are all substantially higher than the ~0.7 nm expected (based on the crystallographic structure [6–10]) for a single layer of $MoSe_2$. Unexpectedly large TMDC heights are commonly measured with AFM [1, 17, 20, 24, 25], and suggest either that the sample is multilayer, or that it has overlayer or underlayer contamination. Distinguishing which of these cases is true requires further careful exploration, as will be discussed below. The apparent step height between L1 and L2 in the nc-AFM image becomes consistent with a 0.7 nm monolayer when electrostatic forces are compensated with KPFM. Notably, however, the surface roughness of the sample measured with each AFM mode is also much larger than the atomic-scale roughness expected for clean $MoSe_2$ flakes. The line scan in the inset of figure 1(d) shows an example of the surface roughness: On the SiO_2 substrate, the roughness is sub-nanometer, whereas on Flake 1 the roughness is greater than 2 nm. Roughness characterizations of each AFM mode, shown on page 5 of the Supplementary Materials, yield similar results. This suggests that the sample has a rough overlayer or underlayer, or is highly defective. Such a layer may have been left behind during sample fabrication.

A location where Flake 1 is folded, shown in the tapping mode data in figure 1(b), is measured with tapping mode AFM in order to directly compare the AFM height to the PL spectrum measured at this location. (PL spectroscopy measurements are presented in section 2.3 of this work.) Note that the height of the fold could not be accurately determined using the area averaging method described on page 3 of the Supplementary Material, since the fold is too small. The height measurements from the line trace only are shown in the figure 1(b) inset. The nonuniformity of this fold could further indicate the presence of an overlayer or underlayer between the bottom layer and the substrate which is not present between stacked layers.

The most notable electrostatic feature is L4 on Flake 2, shown in figures 1(f)–(g): With nc-AFM, L4 is several nanometers high, whereas with KPFM compensation L4 is indistinguishable within the surface roughness from L3. The features comprising L4, which could be either on top of or underneath Flake 2, remained unchanged in shape and location even after the sample was annealed several times at 130 °C in UHV for eight hours. L4 could be surface contamination introduced during the sample fabrication procedure: Selenium-based TMDCs that have been mechanically exfoliated under ambient conditions have been shown to be highly susceptible to airborne contaminants which are mobile on the surface and aggregate to larger patches with average height of 2.2 nm over 45 h, influencing the apparent monolayer height and interlayer spacing [21].

2.2. Raman spectroscopy

Figure 2 presents the Raman response recorded on various regions of Flake 1, labeled in figure 1(a), in the 220–270 cm^{-1} range of the A1g phonon mode. For both CVD-grown and mechanically exfoliated $MoSe_2$, this peak occurs between 239 and 242 cm^{-1} [28, 33, 45, 46]. The side peak at 250 cm^{-1}, also consistent with existing work on both CVD-grown and exfoliated $MoSe_2$ [33, 45, 46], follows the same A-type symmetry as the A1g mode, but is thickness-independent, and its physical origin is unknown [33].

As reported previously, the intensity of the A1g peak (243 cm^{-1}), related to out-of-plane vibrations of Se atoms [28], is found to vary significantly with $MoSe_2$ thickness [33]. Figure 2(a) shows a strong increase of the A1g intensity from position 6 (grey) to position 2 (purple), while no peak could be detected on the thinnest part of the flake (position 1, blue). The spectra acquired in three different regions (figure 2(b), blue) are indistinguishable from the SiO_2 spectrum, confirming that no Raman signal is detected on the thinnest part of Flake 1. However, surprisingly, a strong Raman peak was detected on the folded region of Flake 1 (green, see figure 1(b)).

Raman spectroscopy is often used to determine layer numbers of TMDC samples. In $MoSe_2$, the A1g shift, on the order of 1 cm^{-1} [45], may provide a good estimation of the sample thickness, although it remains close to the spectral resolution. The A1g mode intensity can also be used to determine the number of layers but it is not always detected on few-layers crystals as demonstrated here. Therefore, Raman spectroscopy alone cannot be used to determine layer numbers of $MoSe_2$, so other microscopies, such as AFM and PL spectroscopy, must be relied upon to determine the thickness of $MoSe_2$ crystals.

2.3. Photoluminescence spectroscopy

The results of characterization using PL spectroscopy of Flake 1 and Flake 2 are shown in figure 3. The signal measured at the center of Flake 1 (figure 3(a), blue) is no greater than the SiO_2 background signal. PL spectra were taken at several positions on Flake 1, and were consistent with the results shown in figure 3(a). This quenching could be due to the presence of a water film between the SiO_2 and $MoSe_2$ or the presence of adsorbates from the fabrication process; Similar PL signal quenching has been observed for exfoliated MoS_2 monolayers, and it was determined to be caused by intercalated water between the substrate and the MoS_2 [13, 47]. This quenching cannot be due to the indirect bandgap of multilayer $MoSe_2$,

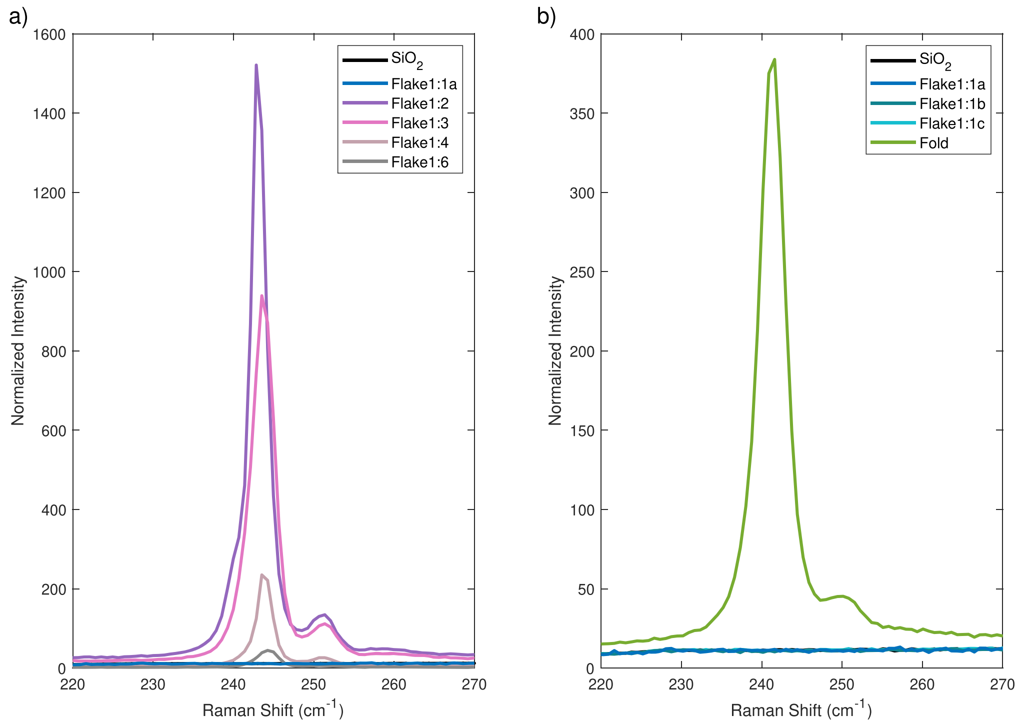

Figure 2. Raman spectroscopy data from Flake 1 at the positions indicated in figure 1(a). (a) shows the Raman spectra taken at the stepped region of Flake 1, where the Flake 1 order stepping up from the substrate is SiO_2 (black, flat), 1(a) (blue, flat), 2 (purple, largest peak), 3 (pink), 4 (rose), 6 (grey, smallest peak). (b) shows Raman spectra at three locations on Flake 1 (1(a), 1(b), and 1c, all blue) which all overlap with the reference measurement taken on SiO_2 (black). (b) also shows the Raman spectrum of the fold (green).

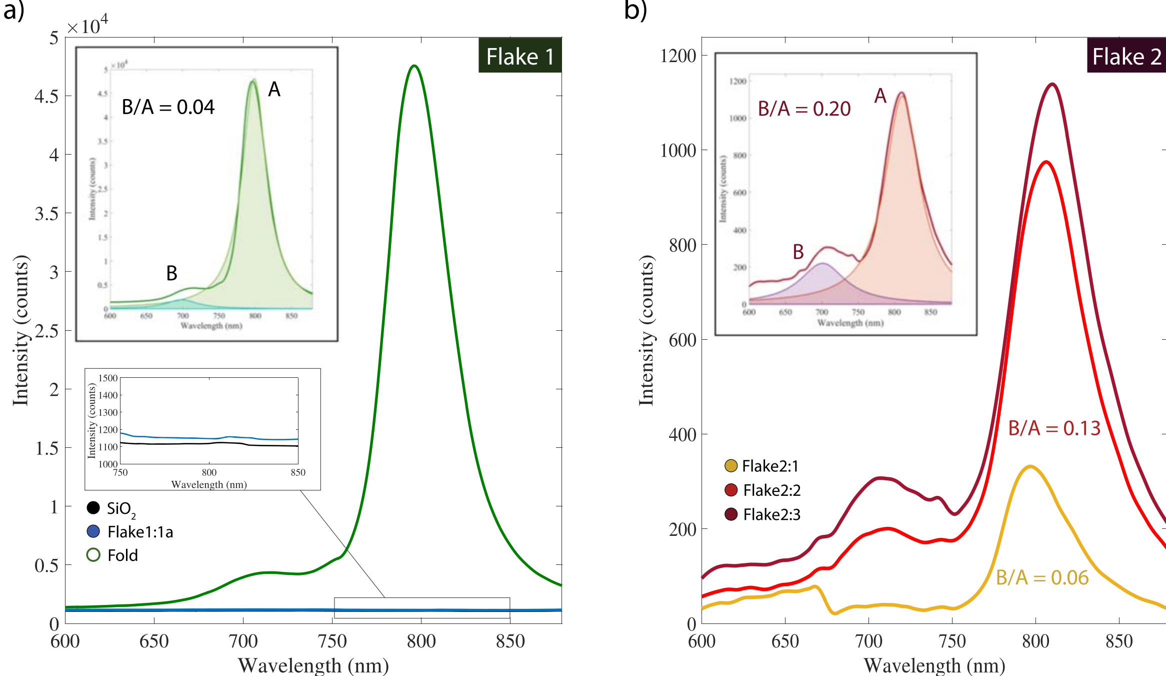

Figure 3. PL spectroscopy data from Flake 1 (a) and Flake 2 (b) with insets showing peak fits from the sum of two Lorentzian functions to extract the B/A ratio. The full details of the fittings can be found on page 5 of the Supplementary Materials. The blue line in (a) shows there is no peak detected at the center of Flake 1, however a strong peak is observed at (798 ± 2) nm where the flake has a fold (black line). The PL spectra from Flake 2 in (b) were taken at the locations indicated in figure 1(e). Flake 2 showed main peaks at (801 ± 3) nm (i), (808 ± 3) nm (ii) and (810 ± 4) nm (iii), with a shift towards a higher intensity but lower energy as the number of layers increases from right to left.

since a PL signal was observed on the fold, which as may be seen in the inset of figure 1(b) is thicker than the Flake 1 center. Previously reported weak PL intensities [37, 48], or peak broadening have also been thought to be caused by aging effects such as oxidation and contamination of adsorbates [49]. A high intensity peak (figure 3(a), green) was detected at the corner of Flake 1 where a fold is visible in figures 1(a) and (b). The PL peak from this fold lies at a wavelength of 798 ± 2 nm. This agrees with the predicted position, peak shape and linewidth that have been reported for both a monolayer [28, 37] and a bilayer data [20]. Depending on the degree of coupling with the underlying layer [37, 50], the fold could be behaving as a suspended monolayer with contributions from a bilayer signal.

The dominant peak at 800 nm is the A-exciton (ground state exciton) contribution [14, 34], and a second smaller peak is present at ~91 nm below (i.e. at ~200 meV higher energy), which corresponds to the B-exciton (higher spin-orbit split state). The ratio of the intensities of the A and B peak is linked to the number of defects in the sample, where a higher B/A ratio indicates higher defect density [34]. Fitting the data from the fold in figure 3(a) with the sum of two Lorentzian peaks, we obtain the results shown in the inset. The B/A ratio is 0.04, suggesting a relatively high defect density compared to the values measured by K. McCreary *et al* [34], where the highest B/A ratio observed for $MoSe_2$ monolayers synthesized by CVD was 0.025.

The PL spectra acquired at three positions on Flake 2 are shown in figure 3(b). The approximate position of the center of the laser beam corresponding to these three positions are labelled in figure 1(e). Since the laser beam area was larger than the individual steps in the flake, the measured peaks are expected to be a convolution of contributions from the different layers. The spectrum at position 1 (yellow) has the A peak at (801 ± 3) nm, in agreement with the peak position of the fold in figure 3(a), and hence of a monolayer as observed in [28, 37]. As the spot moves over the island from right to left, the peak position shifts towards 810 nm, as expected for an increasing number of layers [15, 20, 28]. The B/A ratio increases as the number of layers increases from right to left, and the top layer has a very high ratio of 0.20. Here, we do not see the intensity decreasing as the number of layers increases. This could be due decoupling of the layers [29] but is also likely influenced by the fact that the laser beam spot is large and hence also partly covers the SiO_2 in, for example, the measurement at position 1, and hence sees a smaller contribution from $MoSe_2$. The sudden drop at 675 nm was due to a random fluctuation in the background signal during the PL measurement. The results demonstrate how the presence of water and/or defects that are not visible optically can affect the PL peaks, highlighting the importance of thorough spatial characterization at the nm-scale in order to uncover the quality of the sample.

3. Conclusion

$MoSe_2$ flakes transferred onto SiO_2 were characterized using optical microscopy, Raman spectroscopy, PL spectroscopy and three modes of AFM. The approach typically used to count the number of layers in a TMDC sample is to combine an optical measurement with AFM data. Here we have shown that great care must be taken when using these methods, when determining the number of layers as any one method alone can lead to an incorrect or incomplete characterization of the sample. Furthermore, different methods can lead to contradictory conclusions in terms of the number of TMDC layers present. Future work could be aimed at understanding what type of defects, contamination or processing methods lead to a more reliable and robust layer number determination technique.

4. Methods

$MoSe_2$ layers were exfoliated onto SiO_2 using all-dry viscoelastic stamping. This process uses mechanical exfoliation to transfer 2D crystals onto a viscoelastic Gelfilm stamp, which in turn is pressed against the desired substrate to transfer the flakes onto the surface [26]. Optical microscopy images were obtained using a Nikon optical microscope (Nikon Eclipse LV150N) in reflective mode with a 50x times magnification objective. Tapping mode measurements were performed in air with a MFP3D (BIO) Asylum microscopy using 240C-PP OPUS tips with 1–2 N m^{-1} spring constant and oscillation amplitudes between 14 and 16 nm. nc-AFM and KPFM measuremens were performed in ultrahigh vacuum after having been annealed at 130 °C for 8 h with a modified JEOL JSPM-4500A UHV surface science system at room temperature, using Nanosensors platinum-iridium coated silicon tips with resonant frequency 330 kHz and spring constant 42 N m^{-1}. PL spectra were measured at room temperature using a 532 nm excitation wavelength with a power of 150 μW power and 30s exposure time. Raman spectra were measured using a laser wavelength of 532 nm with power 500 μW and 120 s exposure time. A 100X objective was used to focus the laser beam on the sample, and the beam spot size for PL and Raman measurements was ~1 μm in diameter.

Acknowledgments

The authors thank Philipp Nagler for the fabrication of the $MoSe_2$ sample and the acquisition of the optical microscopy image at Universität Regensburg. Funding from NSERC and FRQ-NT are gratefully acknowledged.

Data availability statement

The data that support the findings of this study are openly available at the following URL/DOI: https://doi.org/10.6084/m9.figshare.16611583.v1.

ORCID iDs

Megan Cowie https://orcid.org/0000-0003-0760-2525

Rikke Plougmann https://orcid.org/0000-0002-0060-642X
Peter Grütter https://orcid.org/0000-0003-1719-8239

References

[1] Li C, Cao Q, Wang F, Xiao Y, Li Y, Delaunay J J and Zhu H 2018 Engineering graphene and TMDs based van der Waals heterostructures for photovoltaic and photoelectrochemical solar energy conversion *Chem. Soc. Rev.* **47** 4981–5037
[2] Das S, Pandey D, Thomas J and Roy T 2019 The Role of Graphene and Other 2D Materials in Solar Photovoltaics *Adv. Mater.* **31** 1802722
[3] Eftekhari A 2017 Molybdenum diselenide ($MoSe_2$) for energy storage, catalysis, and optoelectronics *Appl. Mater. Today* **8** 1–17
[4] Wang Q H, Kalantar-Zadeh K, Kis A, Coleman J N and Strano M S 2012 Electronics and optoelectronics of two-dimensional transition metal dichalcogenides *Nat. Nanotechnol.* **7** 699–712
[5] Le C T, Clark D J, Ullah F, Senthilkumar V, Jang J I, Sim Y, Seong M J, Chung K H, Park H and Kim Y S 2016 Nonlinear optical characteristics of monolayer $MoSe_2$ *Ann. Phys.* **528** 1–9
[6] James P B and Lavik M T 1963 The crystal structure of $MoSe_2$ *Acta Cryst.* **16** 1183
[7] Tomm Y and Fiechter S 2005 Crystal growth of materials for photovoltaics *J. Ceram. Process. Res.* **6** 141–5 (http://www.jcpr.or.kr/journal//doi.html?vol=006&no=02&page=141)
[8] Mahatha S K, Patel K D and Menon K S R 2012 Electronic structure investigation of MoS_2 and $MoSe_2$ using angle-resolved photoemission spectroscopy and abinitio band structure studies *J. Phys.: Condens. Matter* **24** 475504
[9] Roy A, Movva H C P, Satpati B, Kim K, Dey R, Rai A, Pramanik T, Guchhait S, Tutuc E and Banerjee S K 2016 Structural and electrical properties of $MoTe_2$ and $MoSe_2$ grown by molecular beam epitaxy *ACS Appl. Mater. Interfaces* **8** 7396–402
[10] Jiang F, Zhao W-S and Zhang J 2020 Mini-review: Recent progress in the development of $MoSe_2$ based chemical sensors and biosensors *Microelectron. Eng.* **225** 111279
[11] Choi W, Choudhary N, Han G H, Park J, Akinwande D and Lee Y H 2017 Recent development of two-dimensional transition metal dichalcogenides and their applications *Mater. Today* **20** 116–30
[12] Zhang H *et al* 2017 Optical thickness identification of transition metal dichalcogenide nanosheets on transparent substrates *Nanotechnology* **28** 164001
[13] Pollmann E, Madauß L, Schumacher S, Kumar U, Heuvel F, vom Ende C, Yilmaz S, Güngörmüs S and Schleberger M 2020 Apparent differences between single layer molybdenum disulphide fabricated via chemical vapour deposition and exfoliation *Nanotechnology* **31** 15505604
[14] Lu X *et al* 2014 Large-area synthesis of monolayer and few-layer $MoSe_2$ films on SiO_2 substrates *Nano Lett.* **14** 2419–25
[15] Wang S, Wang G, Yang X, Yang H, Zhu M, Zhang S, Peng G and Li Z 2019 Synthesis of monolayer $MoSe_2$ with controlled nucleation via reverse-flow chemical vapor deposition *Nanomaterials* **10** 75
[16] Wang X *et al* 2014 Chemical vapor deposition growth of crystalline monolayer $MoSe_2$ *ACS Nano* **8** 5125–31
[17] Ottaviano L *et al* 2017 Mechanical exfoliation and layer number identification of MoS_2 revisited *2D Mater.* **4** 045013
[18] Larentis S, Fallahazad B and Tutuc E 2012 Field-effect transistors and intrinsic mobility in ultra-thin $MoSe_2$ layers *Appl. Phys. Lett.* **101** 223104
[19] Tongay S *et al* 2013 Defects activated photoluminescence in two-dimensional semiconductors: Interplay between bound, charged, and free excitons *Sci. Rep.* **3** 2657
[20] Sha Y, Xiao S, Zhang X, Qin F and Gu X 2017 Layer-by-layer thinning of $MoSe_2$ by soft and reactive plasma etching *Appl. Surf. Sci.* **411** 182–8
[21] Pürckhauer K, Kirpal D, Weymouth A J and Giessibl F J 2019 Analysis of airborne contamination on transition metal dichalcogenides with atomic force microscopy revealing that sulfur is the preferred chalcogen atom for devices made in ambient conditions *ACS Appl. Nano Mater.* **2** 2593–8
[22] Qi J, Lan Y-W, Stieg A Z, Chen J-H, Zhong Y-L, Li L-J, Chen C-D, Zhang Y and Wang K L 2014 Piezoelectric effect in chemical vapour deposition-grown atomic-monolayer triangular molybdenum disulfide piezotronics *Nat. Commun.* **6** 7430
[23] Liu H, Xu L, Liu W, Zhou B, Zhu Y, Zhu L and Jiang X 2018 Production of mono- to few-layer MoS_2 nanosheets in isopropanol by a salt-assisted direct liquid-phase exfoliation method *J. Colloid Interface Sci.* **515** 27–31
[24] Li S L, Miyazaki H, Song H, Kuramochi H, Nakaharai S and Tsukagoshi K 2012 Quantitative raman spectrum and reliable thickness identification for atomic layers on insulating substrates *ACS Nano* **6** 7381–8
[25] Haigh S J, Gholinia A, Jalil R, Romani S, Britnell L, Elias D C, Novoselov K S, Ponomarenko L A, Geim A K and Gorbachev R 2012 Cross-sectional imaging of individual layers and buried interfaces of graphene-based heterostructures and superlattices *Nat. Mater.* **11** 764–7
[26] Castellanos-Gomez A, Buscema M, Molenaar R, Singh V, Janssen L, Van Der Zant H S J and Steele G A 2014 Deterministic transfer of two-dimensional materials by all-dry viscoelastic stamping *2D Mater.* **1** 011002
[27] Nagler P *et al* 2017 Interlayer exciton dynamics in a dichalcogenide monolayer heterostructure *2D Mater.* **4** 025112
[28] Tonndorf P *et al* 2013 Photoluminescence emission and Raman response of monolayer MoS_2, $MoSe_2$, and WSe_2 *Opt. Express* **21** 4908–16
[29] Arora A, Nogajewski K, Molas M, Koperski M and Potemski M 2015 Exciton band structure in layered $MoSe_2$: From a monolayer to the bulk limit *Nanoscale* **7** 20769–75
[30] Wang Y-P, Zhou H-J, Zhao G-H, Xia T-L, Wang L, Wang L and Zhang L-Y 2016 Rapidly counting atomic planes of ultra-thin $MoSe_2$ nanosheets ($1 \leqslant n \leqslant 4$) on SiO_2/Si substrate *Rare Met.* **35** 632–6
[31] Taghavi N S, Gant P, Huang P, Niehues I, Schmidt R, Michaelis de Vasconcellos S, Bratschitsch R, García-Hernández M, Frisenda R and Castellanos-Gomez A 2019 Thickness determination of MoS_2, $MoSe_2$, WS_2 and WSe_2 on transparent stamps used for deterministic transfer of 2D materials *Nano Res.* **12** 1691–5
[32] Wu J-P, Wang L and Zhang L-Y 2017 Rapid and nondestructive layer number identification of two-dimensional layered transition metal dichalcogenides *Rare Met.* **36** 698–703
[33] Soubelet P, Bruchhausen A E, Fainstein A, Nogajewski K and Faugeras C 2016 Resonance effects in the Raman scattering of monolayer and few-layer $MoSe_2$ *Phys. Rev.* B **93** 155407
[34] McCreary K M, Hanbicki A T, Sivaram S V and Jonker B T 2018 A- and B-exciton photoluminescence intensity ratio as a measure of sample quality for transition metal dichalcogenide monolayers *APL Mater.* **6** 111106
[35] Kumar N, Cui Q, Ceballos F, He D, Wang Y and Zhao H 2014 Exciton diffusion in monolayer and bulk $MoSe_2$ *Nanoscale* **6** 4915–9
[36] Silva J P B, Almeida Marques C, Viana A S, Santos L F, Gwozdz K, Popko E, Connolly J P, Veltruská K, Matolín V and Conde O 2020 Morphological, optical and

photovoltaic characteristics of $MoSe_2/SiO_x/Si$ heterojunctions *Sci. Rep.* **10** 1–9
[37] Tongay S, Zhou J, Ataca C, Lo K, Matthews T S, Li J, Grossman J C and Wu J 2012 Thermally driven crossover from indirect toward direct bandgap in 2D semiconductors: $MoSe_2$ versus MoS_2 *Nano Lett.* **12** 5576–80
[38] Sadewasser S, Carl P, Glatzel T and Lux-Steiner M C 2004 Influence of uncompensated electrostatic force on height measurements in non-contact atomic force microscopy *Nanotechnology* **15** 14
[39] Sadewasser S and Ch Lux-Steiner M 2003 Correct height measurement in noncontact atomic force microscopy *Phys. Rev. Lett.* **91** 266101
[40] Melitz W, Shen J, Kummel A C and Lee S 2011 Kelvin probe force microscopy and its application *Surf. Sci. Rep.* **66** 1–27
[41] Voigtländer B 2019 *Atomic Force Microscopy* vol 65 (Switzerland: Springer Publishing) ch 9–10
[42] Sadewasser S and Glatzel T 2018 *Kelvin Probe Force Microscopy* vol 65 (Switzerland: Springer Publishing) ch 2
[43] Li H, Wu J, Huang X, Lu G, Yang J, Lu X, Xiong Q and Zhang H 2013 Rapid and reliable thickness identification of two-dimensional nanosheets using optical microscopy *ACS Nano* **7** 10344–53
[44] Cowie M, Plougmann R, Schumacher Z and Grütter P 2021 Single-dopant band bending fluctuations in $MoSe_2$ measured with electrostatic force microscopy *Mesoscale and Nanoscale Physics* arXiv:2109.15275
[45] O'Brien M, McEvoy N, Hanlon D, Lee K, Gatensby R, Coleman J N and Duesberg G S 2015 Low wavenumber Raman spectroscopyof highly crystalline $MoSe_2$ grown bychemical vapor deposition *Phys. Status Solidi* b **252** 2385–9
[46] Kim K, Lee J-U, Nam D and Cheong H 2016 Davydov splitting and excitonic resonance Effects in Raman spectra of few-layer $MoSe_2$ *ACS Nano* **10** 8113–20
[47] Varghese J O, Agbo P, Sutherland A M, Brar V W, Rossman G R, Gray H B and Heath J R 2015 The influence of water on the optical properties of single-layer molybdenum disulfide *Adv. Mater.* **27** 2734–40
[48] Jadczak J, Kutrowska-Girzycka J, Kapuściński P, Huang Y S, Wójs A and Bryja L 2017 Probing of free and localized excitons and trions in atomically thin WSe_2, WS_2, $MoSe_2$ and MoS_2 in photoluminescence and reflectivity experiments *Nanotechnology* **28** 395702
[49] Gao J, Li B, Tan J, Chow P, Lu T-M and Koratkar N 2016 Aging of transition metal dichalcogenide monolayers *ACS Nano* **10** 2628–35
[50] Froehlicher G, Lorchat E and Berciaud S 2018 Charge versus energy transfer in atomically thin graphene-transition metal dichalcogenide van der waals heterostructures *Phys. Rev.* X **8** 011007

Supplementary Materials

Optical microscopy contrast measurements

From the optical microscopy image of the sample, the contrast difference between the substrate and the $MoSe_2$ flakes can indicate the number of layers stacked [1]. Figure S1 shows the contrast data for a selected region of the sample that includes Flake 1. The images were analysed according to the method in [1] using ImageJ and MATLAB. The contrast values at location 1 (Flake 1) from the color and red channels (values -9.7 and -35.4) are similar to the contrast values observed for monolayers of MoS_2 (Fig. 5 in [1]) and WSe_2 (Fig. 7 in [1]) on 300 nm of SiO_2/Si in [1].

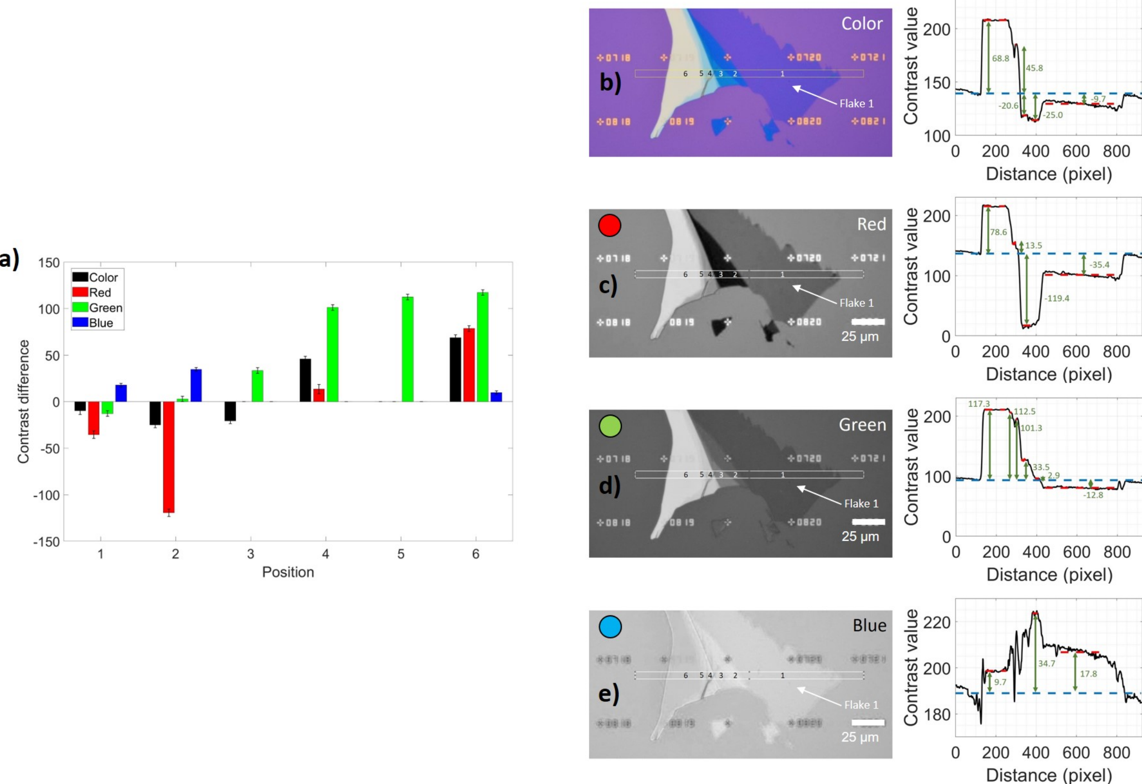

Figure S1: Optical microscopy images and contrast profiles. The contrast difference between each position along the region shown by the white outline in b)-e) and the substrate were calculated following the procedure in [1] and summarised in a). Figures b)-e) show the color, red, green and blue channels of the optical microscopy image, with the corresponding intensity line profile from the indicated region. In each contrast profile graph, the substrate contrast is labelled with a blue dashed line. The contrast value at each position was obtained by averaging the data at locations labelled by the red dashed lines.

AFM height measurements

For all of the AFM data shown in this work, height measurements were found by averaging over large sample areas. This, as opposed to measuring individual line profiles, is a more robust way of determining the height, particularly if the sample surface is rough. First, the z-channel image is leveled until the width of a histogram of the entire substrate area is equal to the measurement noise. Then, Gaussean fits (of the form $f = a \times exp\left(\frac{-(z-b)}{c}\right)^2$) are found for each sample area. b gives the mean z-channel value and $\sigma = \frac{c}{\sqrt{2}}$ gives the uncertainty of the z-channel value. The substrate mean was subtracted from each sample area mean to determine the sample area height ($h = b_{sample} - b_{substrate}$). Uncertainties were found by adding the Gaussean fit widths in quadrature as $\delta h = \sqrt{(\sigma_{sample})^2 + (\sigma_{substrate})^2}$. Figure S2 shows an example of the masks and histograms used to evaluate the first layer height measured using ncAFM, where Figure S2a and b show the substrate mask, histogram, and fit, and c and d show the first layer mask, histogram, and fit. The AFM height results are shown in Figure **??**(h-i), and a summary is presented in tabular form in Table 1.

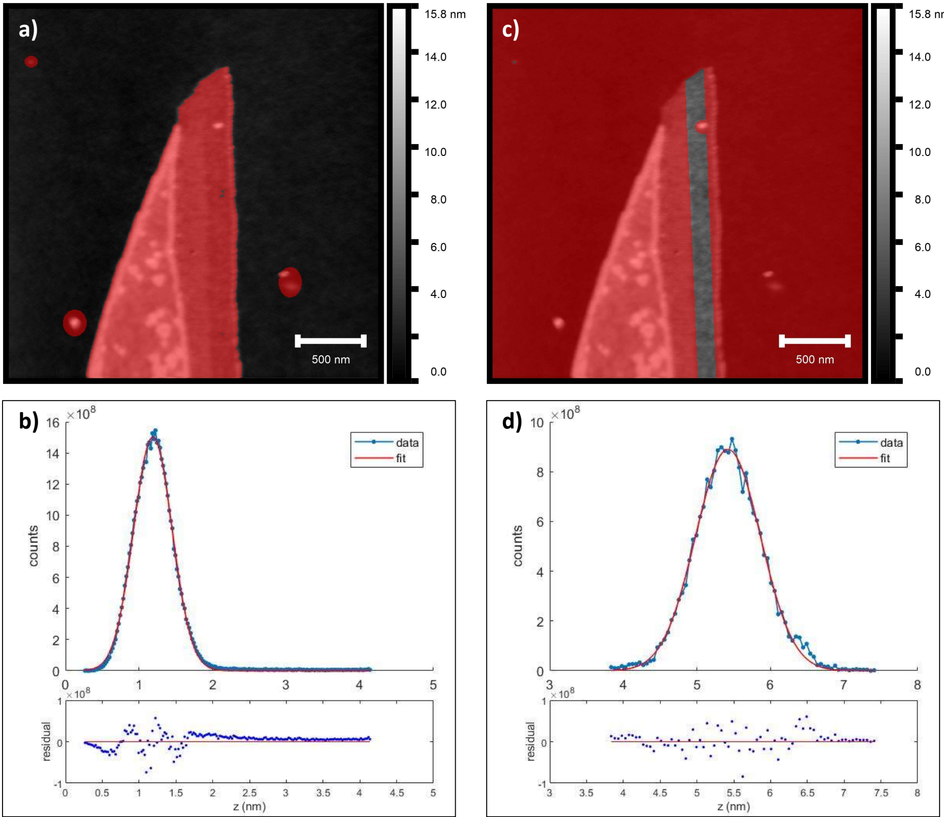

Figure S2: An example of the procedure used to extract heights from AFM data. The total substrate area was masked (a), binned, and fit (b), as was one region of the sample (c-d). The fit means were then subtracted to give the sample region height.

Location	Method	Height (nm)
Flake 1		
Substrate	Tapping Mode	0.0 ± 0.5
	NC-AFM	0.0 ± 1.6
	KPFM	0.0 ± 0.5
1st layer	Tapping Mode	6.5 ± 1.5
	NC-AFM	6.0 ± 1.9
	KPFM	3.9 ± 0.6
Flake 2		
Substrate	Tapping Mode	0.0 ± 0.3
	NC-AFM	0.0 ± 0.4
	KPFM	0.0 ± 0.2
1st layer	Tapping Mode	3.5 ± 0.6
	NC-AFM	4.2 ± 0.5
	KPFM	3.1 ± 0.5
2nd layer	Tapping Mode	4.1 ± 0.6
	NC-AFM	5.4 ± 0.5
	KPFM	3.6 ± 0.4
3rd layer	Tapping Mode	5.8 ± 0.5
	NC-AFM	7.9 ± 0.9
	KPFM	8.4 ± 0.4
4th layer	Tapping Mode	7.8 ± 0.8
	NC-AFM	10.9 ± 1.1
	KPFM	9.0 ± 0.4

Table 1: Summary of the $MoSe_2$ heights measured with tapping mode AFM, NC-AFM, and KPFM for each region defined in Figure 1.

AFM surface roughness measurements

The surface roughness was measured using Gwyddion by masking the various regions of the sample (as in Figure S2) and measuring the root mean square (RMS) roughness. (Note that these roughness values very closely agree with the height uncertainties found by taking the histogram width of each layer, shown in Table 2.)

Location	Method	RMS Roughness (nm)
Flake 1		
Substrate	Tapping Mode	0.4
	NC-AFM	1.1
	KPFM	0.4
1st layer	Tapping Mode	1.7
	NC-AFM	1.1
	KPFM	0.7
Flake 2		
Substrate	Tapping Mode	0.2
	NC-AFM	0.3
	KPFM	0.2
1st layer	Tapping Mode	0.6
	NC-AFM	0.5
	KPFM	0.4
2nd layer	Tapping Mode	0.6
	NC-AFM	0.6
	KPFM	0.5
3rd layer	Tapping Mode	0.4
	NC-AFM	0.6
	KPFM	0.3
4th layer	Tapping Mode	0.8
	NC-AFM	1.2
	KPFM	0.4

Table 2: RMS roughnesses measured with tapping mode AFM, NC-AFM, and KPFM for each region defined in Figure 1.

Photoluminescence measurements

The photoluminescence spectra in Figure 2 were analyzed and plotted in MATLAB. To remove random background noise artefacts in the data, the spectra were cleaned up using the function smooth(data,0.05,'rloess'), a local regression using weighted linear least squares and a 2nd degree polynomial model. Lower weight is assigned to outliers in the regression; the method assigns zero weight to data outside six mean absolute deviations. The data was smoothed using this method using a span of 5% of the total number of data points. The background signal from the SiO_2 was subtracted from the $MoSe_2$ curves. The peak position and associated uncertainty were obtained as follows: The main peaks were fitted to a Lorentzian function $f(x) = A/(1+((x-x_0)/\gamma)^2)$, where A is the height of the peak, x_0 is the position of the peak (wavelength), and γ is the width of the peak at half maximum [2]. The fitting was carried out in MATLAB (using fit function), with the appropriate starting parameters estimated. The error in the x_0 peak

locations was found by forcibly varying x_0 around the fitted output value (while letting A and γ vary), to find the range of x_0 for which the coefficient of determination (r-squared) value of the fit stayed within 0.01 of its optimum. R-squared indicates the proportionate amount of variation in the response variable y explained by the independent variables x in the linear regression model. The larger the r-squared is, the more variability is explained by the linear regression model. R-squared is the proportion of the total sum of squares explained by the model: $R_2 = SSR/SST = 1 - SSE/SST$ where SSR is the sum of squared regression, SST is the sum of squared total, and SSE is the sum of squared error.

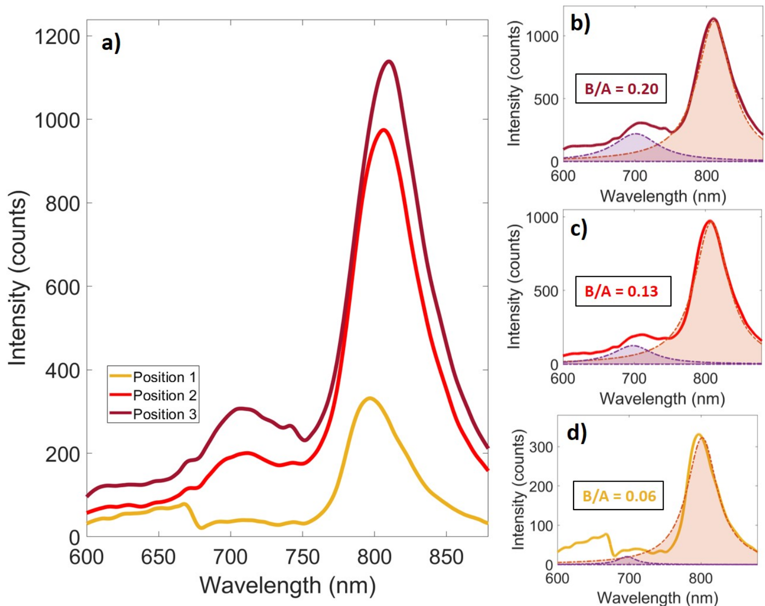

Figure S3: Two peak Lorentzian curve fittings for positions 1, 2 and 3 on Flake 2. The ratio in intensity between the B and A peak is given for each spectrum.

References

[1] Hai Li, Jumiati Wu, Xiao Huang, Gang Lu, Jian Yang, Xin Lu, Qihua Xiong, and Hua Zhang. Rapid and reliable thickness identification of two-dimensional nanosheets using optical microscopy. *ACS Nano*, 7(11):10344–10353, 11 2013.

[2] Kathleen M. McCreary, Aubrey T. Hanbicki, Saujan V. Sivaram, and Berend T. Jonker. A- and B-exciton photoluminescence intensity ratio as a measure of sample quality for transition metal dichalcogenide monolayers. *APL Materials*, 6(11):111106, 11 2018.